# Quantification of flexural fatigue life and 3D damage in carbon fibre reinforced polymer laminates

Zhe Liu [1], Peifeng Li [1,] *, Narasimalu Srikanth [2], Tong Liu [3], Gin Boay Chai [1]

[1] School of Mechanical and Aerospace Engineering, Nanyang Technological University, Singapore

[2] Energy Research Institute @NTU, Nanyang Technological University, Singapore

[3] Singapore Institute of Manufacturing Technology, Singapore

* Corresponding author's email: peifeng.li@ntu.edu.sg (P. Li); Tel: +65 6790 4766.

## Abstract

Carbon fibre reinforced polymer (CFRP) laminated composites have become attractive in the application of wind turbine blade structures. The cyclic load in the blades necessitates the investigation on the flexural fatigue behaviour of CFRP laminates. In this study, the flexural fatigue life of the $[+45/-45/0]_{2s}$ CFRP laminates was determined and then analysed statistically. X-ray microtomography was conducted to quantitatively characterise the 3D fatigue damage. It was found that the fatigue life data can be well represented by the two-parameter Weibull distribution; the life can be reliably predicted as a function of applied deflections by the combined Weibull and Sigmodal models. The delamination at the interfaces in the 1$^{st}$ ply group is the major failure mode for the flexural fatigue damage in the CFRP laminate. The calculated delamination area is larger at the interfaces adjacent to the 0 ply. The delamination propagation mechanism is primarily matrix/fibre debonding and secondarily matrix cracking.

*Keywords*: A. Laminates; B. Fatigue; B. Delamination; D. Radiography.

# 1 Introduction

Fibre reinforced polymer (FRP) laminated composites have been widely used in wind turbine blade structures due to their good strength-to-weight ratio, corrosion resistance and excellent fatigue properties [1-3]. Glass fibres are currently the most common reinforcements in the laminate for wind turbine blades; however, there is an increasing interest in carbon fibres as a result of their decreasing cost and better properties. Wind turbine blades in service are subjected to highly variable loads such as aerodynamic, gravitational and inertial forces. The aerodynamic and gravitational forces bring about the cyclic stress in the blade structures, making the flexural fatigue one of the important failure modes in the blades [4, 5]. It is thus necessary to investigate the flexural fatigue behaviour of carbon fibre reinforced polymer (CFRP) laminates in order to predict the service life of the turbine blades subjected to cyclic loading.

The fatigue damage in FRP laminated composites is usually associated with the degradation of stiffness. The stiffness is an indicator for the laminate's resistance capacity to fatigue loads. Note that in force-controlled fatigue, the load bearing capacity of laminates can also be used to describe the fatigue failure when it declines to the level of the applied stress in the fatigue cycle [6]. However, the failure in displacement-controlled fatigue is often specified when the stiffness degrades to a defined level. The stiffness degradation process is influenced by the laminate constituents, layup sequences, and fatigue loading conditions (such as the load type and level) [7]. Philippidis and Vassilopoulos [8] reported that the reduction of stiffness up to the failure in glass fibre reinforced polymer laminates ranges from less than 7% to 50% for different layup sequences. There seems no general agreement on the stiffness degradation level at which the fatigue failure is defined [8-10]. Jessen et

al. [9] considered the occurrence of failure in the tension-tension fatigue tests of pultruded glass composites when the stiffness reduces by 20%. Jones et al. [10] proposed that a 15% reduction in stiffness of [0/90] epoxy-based laminates serves as the criterion for the flexural fatigue failure. The ISO 13003 standards suggested the stiffness reduction between 5% and 20% for the fatigue failure in FRP composites. Therefore, it is worthwhile to analyse the stiffness degradation behaviour in CFRP laminated composites subjected to flexural fatigue loads for the prediction of fatigue life.

The fatigue life of FRP laminates is usually scattered even under carefully controlled testing conditions because of the inhomogeneous microstructure and anisotropic properties. Various statistical methods have been developed to analyse the distribution of fatigue life data [11-13]. Among these methods, Weibull distribution function has been well-established to characterise the fatigue life of laminated composites [11]. However, to design laminate components requires statistically predicting the fatigue life as a function of cyclic loading levels.

The fatigue failure mechanism of FRP composites are generally complicated and in the forms of matrix cracks, fibre failure, matrix/fibre debonding and delamination [14]. However, one of these failure modes can be the dominant mechanism responsible for the fatigue damage in the composite depending on the material and loading conditions [15, 16]. It is thus essential to examine the damage in the laminate during and after the fatigue test and to determine how the damage leads to the degradation of properties. X-ray microtomography (μXT) has recently become a powerful non-destructive testing technique to characterise the full 3D material damage under various loads [17-20]. In particular, the failure mechanisms of FRP composites subjected to various loads have been reliably investigated using the μXT

technique [14, 21-23]. Nevertheless, a quantitative analysis of the 3D damage has been rarely reported on CFRP composites [21].

The aim of this study was to investigate the stiffness degradation, fatigue life prediction and 3D damage of CFRP laminates with the symmetric layup sequence $[+45/-45/0]_{2s}$ subjected to flexural fatigue loads. Static three-point bending flexural tests were conducted to measure the elastic modulus and failure strength/deflection of the laminate. Displacement-controlled flexural fatigue tests in the three-point bending fixture were performed on the laminate specimens at different cyclic deflection levels to determine the stiffness degradation process and the fatigue life. The two-parameter Weibull distribution model was employed to analyse and predict the fatigue life. Finally, the 3D damage in the laminate after a specific fatigue cycle was characterised in the μXT, and the interlaminar facture surfaces after the fatigue tests were examined in the scanning electron microscope (SEM). The statistical method and the μXT technique provided the insights into the flexural fatigue life and 3D damage in the CFRP laminate.

## 2 Experimental procedure

### *2.1 Materials and specimens*

The carbon fibre reinforced polymer laminates with the symmetric layup sequence $[+45/-45/0]_{2s}$ were fabricated using the L-930HT (Cytec Solvay Group, USA) flame retardant epoxy carbon prepregs in the unidirectional form. The cured ply thickness of the prepreg is 0.178 mm as provided by the prepreg manufacturer. The $[+45/-45/0]_{2s}$ laminates are extensively used in some components in the wind turbine blade, especially those subjected to multiaxial stresses, such as the skin and the root [1, 2, 14].

The prepreg laminates were cured in the autoclave at 127 °C for 60 min under the vacuum pressure of -0.069 MPa (i.e., 0.069 MPa lower than the atmospheric pressure). The pressure in the chamber was maintained at 0.41 MPa during the entire curing process. The laminates after curing were approximately 2.13 mm in depth (thickness). The rectangular specimens (150×12 mm) for the flexural tests were machined from the cured CFRP laminates using the waterjet cutter. The transverse cross section of the laminate was ground and polished for the optical microscopic examination to inspect any manufacturing defects and determine the fibre volume fraction. Fig. 1 illustrates very few small pores in the +45 ply, suggesting the negligible effect on the flexural fatigue behaviour [24, 25]. The fibre volume fraction was (57.8±2.7) % as measured from the optical images on various locations in the transverse cross section.

## *2.2 Static and fatigue flexural tests*

The flexural experiments with the support span length 75 mm were conducted in an in-house three-point bending fixture which was clamped to the MTS 810 (MTS Systems Corp., USA) servo-hydraulic universal testing machine by the wedge grips. A relatively high span-to-depth ratio of approximately 35 was employed because (1) the high ratio specimen is recommended for the flexural test of highly anisotropic laminated composites and (2) the shear stress effect on the failure behaviour becomes insignificant with the increased span length [25]. Note that the 0 ply in the laminate was directed along the span in the flexural tests.

Four specimens were subjected to the static flexural tests (ASTM D790) with the crosshead velocity 2 mm $min^{-1}$ to determine the flexural properties. After the failure, the crosshead returned to the initial position, and reloading was then applied to the

same specimens to characterise the residual properties. Displacement-controlled flexural fatigue tests with the sinusoidal waveform (ASTM D7774) were performed under five different cyclic deflection levels (CDL). The CDL normalised by the static failure deflection (SFD) was $\gamma_c$ = CDL/SFD = 0.58, 0.65, 0.71, 0.84 and 0.91. Eight specimens were repeated in the flexural fatigue tests under each CDL. The ratio of the minimum and maximum displacement was constant at $R$ = 0.1 for all the fatigue experiments. The frequency was limited to 2 Hz given the large midspan deflection. The stiffness was measured and monitored in the fatigue tests.

## *2.3 X-ray microtomographic and fractographic characterisation*

To characterise the damage, the flexural fatigue test on a CFRP laminate specimen subjected to the normalised CDL $\gamma_c$ = 0.84 was interrupted after the specific cycle. The midspan portion of the specimen was then scanned in the x-ray microtomography at 55 kV and 46 μA [17, 18, 26]. A set of 720 projections were recorded as the specimen was rotated through 360°. The 3D image was reconstructed from the projections using an in-house algorithm that enhances the reconstruction quality of planar objects [27, 28]. The internal damage including the fibre failure, matrix cracking and delamination was visualised in the AVIZO/FIRE software. The ImageJ software was used to quantify the projected area of the delamination in the specimen.

After fatigue testing under each CDL, the interlaminar fracture surfaces of the laminate specimens were examined in the SEM to explore the fatigue failure mechanism.

# 3 Results and discussion

## *3.1 Static flexural behaviour*

The static flexural response of the CFRP laminate was quantitatively characterised by the measured histories of both the bending load $P$ and the midspan deflection $D$. As the deflection of the specimen exceeds 10% of the support span, the flexural stress at the midpoint of the outer surface was approximated with a correction factor (ASTM D790):

$$\sigma = \left(\frac{3PL}{2bd^2}\right)\left(1 + 6\left(\frac{D}{L}\right)^2 - 4\frac{d}{L}\frac{D}{L}\right) \tag{1}$$

where $L$ = 75 mm, $b$ = 12 mm and $d$ = 2.13 mm are the support span, the width and the depth (thickness) of the CFRP laminate, respectively. The flexural strain at the midpoint was calculated as follows.

$$\varepsilon = \frac{6dD}{L^2} \tag{2}$$

Fig. 2 shows the representative flexural stress–strain curve of the CFRP laminate. After the initial linear elastic stage, the stress–strain response is nonlinear with the decreasing slope prior to the static failure deflection SFD at which the stress drops abruptly. The nonlinear feature is primarily due to the viscoelastic nature of the epoxy resin matrix. All the specimens were reloaded to measure the residual modulus and strength (Fig. 2). The typical flexural stress–strain curve for reloading also consists of the initial linear stage and the subsequent nonlinear portion before the flexural stress reaches the peak. Compared to the response for the first loading, the flexural stress is smaller under reloading. However, the strain at the reloading failure is slightly larger probably due to the contribution of residual strains. The flexural stress then gradually decreases with oscillation until the sharp drop of stress.

There are several methods to define the modulus of laminated composites subjected to the static three-point bending load [29]. The initial modulus $E_0$ is defined as the ratio of the flexural stress to the corresponding strain within the initial elastic limit (Fig. 2); thus the $E_0$ can be calculated:

$$E_0 = \frac{L^3}{4bd^3} m \tag{3}$$

where $m$ is the slope of the initial linear portion of the load $P$ versus deflection $D$ curve. The static secant modulus $E_s = \sigma/\varepsilon$ at a specific deflection (e.g., $(E_s)_{0.84}$ for the deflection at 0.84×SDF) is equal to the flexural stress (Eq. 1) divided by the corresponding strain (Eq. 2). The secant modulus varies with the deflection level in the nonlinear portion of the curve.

Table 1 summarises the flexural properties of CFRP laminates subjected to static three-point bending and subsequent reloading. The good repeatability indicates the consistent material fabrication, specimen preparation and experimental setup. Both the residual modulus and the residual strength are lower than the flexural properties. Table 1 also suggests that after failure the laminate can bear approximately 62% of the flexural strength with the residual modulus reduced by nearly 21% of the initial modulus.

## *3.2 Stiffness degradation under flexural fatigue*

The stiffness degradation was monitored in the flexural fatigue tests to assess the fatigue resistance in the CFRP laminate. A convenient method to reflect the stiffness under fatigue is the fatigue secant modulus $E_n$ which is defined by dividing the maximum stress with the corresponding strain in the $n^{th}$ cycle. In the present displacement-controlled flexural fatigue test, the maximum flexural deflection is

constant under each normalised CDL $\gamma_c$, therefore the fatigue secant modulus is proportional to the measured bending load.

Fig. 3 demonstrates the typical normalised stiffness as a function of the number of fatigue cycles under the five different CDL. Note that the stiffness degradation curves are similar with a very small deviation among the eight laminate specimens for each CDL. The fatigue secant modulus $E_n$ was normalised with the modulus $E_1$ in the first cycle instead of the static initial modulus $E_0$, because the secant modulus $E_1$ under each CDL usually differs from the $E_0$ due to the nonlinearity of the laminate (Fig. 2).

The normalised stiffness $E_n/E_1$ decreases with the increasing number of fatigue cycles prior to the final failure (Fig. 3). The rate of stiffness degradation is also significantly affected by the applied CDL. In the laminate subjected to displacement-controlled flexural fatigue loads, the stiffness degradation process can be divided into three stages as follows.

Stage I: a rapid reduction of stiffness by 1–10% occurs within the first several (<5) cycles as a result of micro-cracking in the matrix which may be caused by the presence of very small pores. Note that the applied sinusoidal waveform was slightly tapered in the first several cycles before the predefined CDL was reached, thus leading to the minor fluctuation in stiffness in this stage. Under higher fatigue CDL, the stiffness degrades with a faster rate in the laminate, and more reduction of stiffness is observed.

Stage II: the stiffness continues to degrade with a very low and steady rate due to the evolution of matrix cracks. The effect of the applied CDL on the degradation rate

seems to be insignificant. This stage defines the major life of fatigue of the laminate prior to the rapid reduction of stiffness.

Stage III: the abrupt stiffness degradation represents the severe loss of resistance to flexural fatigue loads. This is caused by the formation of large delamination which is prone to interconnect with the fibre fracture and matrix cracks.

The stiffness degradation in flexural fatigue tests seems different from that in other types of fatigue tests. For instance, the stiffness decreases faster under the lower stress level in the force-controlled tension-compression fatigue tests of CFRP laminates [30].

## *3.3 Flexural fatigue life*

### *3.3.1 Statistical characteristics*

In the flexural fatigue test, the fatigue failure can be defined at the cycle when the stiffness degrades by a specific percentage. It can be assumed that a relative reduction in cyclic stiffness during flexural fatigue tests is equivalent to the percentage reduction in the static flexural modulus [15], e.g., 21% for the $[+45/-45/0]_{2s}$ CFRP laminate as discussed in Section 3.1 (refer to Table 1). In the present study, the fatigue life $N$ is therefore equal to the number of cycles in which the fatigue stiffness decreases by 21%.

The two-parameter Weibull analysis was performed to statistically characterise the flexural fatigue life $N$ of CFRP laminates subjected to three-point bending at a specific normalised CDL $\gamma_c$. The cumulative distribution function $F(N)$ is defined:

$$F(N) = 1 - \exp\left(-\left(\frac{N}{\beta}\right)^{\alpha}\right) \tag{4}$$

where $\alpha$ is the shape parameter (Weibull slope) and $\beta$ is the scale parameter (characteristic life). The graphical method using the Weibull plot is applied to determine the parameters $\alpha$ and $\beta$. Eq. (4) can be expressed in the following natural logarithmic form:

$$\ln\left(-\ln\left(1-F(N)\right)\right)=\alpha\ln(N)-\alpha\ln(\beta) \tag{5}$$

To plot a graph for Eq. (5), the fatigue lives under a specific $\gamma_c$ are rearranged in the ascending order. The empirical cumulative distribution function $F(N_i)$ for the $i^{th}$ fatigue life $N_i$ is determined by the failure probability $P_f$ for this series of lives using Bernard's approximation:

$$F(N_i)=P_f=\frac{i-0.3}{k+0.4} \tag{6}$$

where $k = 8$ is the number of specimens tested under the $\gamma_c$.

As shown in Fig. 4, the expression ln(-ln(1-$F$($N$))) was plotted against the corresponding natural logarithm of fatigue life ln($N$) for each $\gamma_c$ as measured in the tests. The data was fitted using linear regression analysis to calculate the shape parameter $\alpha$ and the scale parameter $\beta$ as listed in Table 2. A good correlation coefficient $R^2$>0.92 was achieved for each $\gamma_c$, thus indicating that the Weibull distribution model can reasonably characterise the statistical nature of the fatigue life of the CFRP laminate. The slope of the line represents the shape parameter, while the characteristic life corresponds to the life at the failure probability $P_f = F(N) = 0.632$ (i.e., 1-1/$e$).

To further validate the Weibull analysis, the Kolmogorov-Smirnov goodness-of-fit statistic $D$ was calculated as follows:

$$D=\max_{i=1}^{k}\left(\left|\frac{i}{k}-F(N_i)\right|\right) \tag{7}$$

where $N_i$ is the $i^{th}$ fatigue failure life in the ascending ordered lives, and $F(N_i)$ denotes the theoretic cumulative distribution as in Eq. (4). As listed in Table 3, the $D$ value for each $\gamma_c$ was compared to the critical value $D_c$ defined in the Kolmogorov-Smirnov table [31]. Since the $D$ is less than the $D_c$ = 0.454 at a 5% level of significance, the two-parameter Weibull analysis can be suitable to predict the life at flexural fatigue failure of the CFRP laminate.

### *3.3.2 Prediction of fatigue life*

The failure probability $P_f$ is an important parameter to evaluate the fatigue behaviour of laminates. Substituting $P_f = F(N)$ into Eq. (4), the fatigue life can be predicted as a function of the failure probability using the shape and scale parameters ($\alpha$ and $\beta$) for each normalised CDL $\gamma_c$:

$$N = \exp\left(\frac{\ln\left(-\ln\left(1-P_f\right)\right)+\alpha\ln\left(\beta\right)}{\alpha}\right) \tag{8}$$

The median fatigue lives ($P_f$ = 0.5), the characteristic lives ($P_f$ = 0.632) and the fatigue lives for the failure probability $P_f$ = 0.95 were thus calculated for all the five $\gamma_c$ (refer to Fig. 5).

For a specific failure probability $P_f$, the fatigue life $N$ degrades with the increasing $\gamma_c$. A Sigmoidal model was used to quantify the relation between the normalised CDL $\gamma_c$ and the common logarithm of life log($N$):

$$\gamma_c = \frac{A_1 - A_2}{1+\exp\left(\left(\log(N)-N_0\right)/\Delta N\right)} + A_2 \tag{9}$$

where $A_1$, $A_2$, $N_0$ and $\Delta N$ are the constants. The $\gamma_c$ was regressed against the log($N$) for the $P_f$ = 0.5, 0.632, and 0.95. The statistical correlation coefficient $R^2$ for each $P_f$ is >0.98, thus implying that the Sigmoidal model can well represent the variation of flexural fatigue life with the applied deflection level. The Sigmoidal model has been

extensively applied to describe the growth mode in biological science, and has also been employed to predict the fatigue life of 25° braided composites [29].

### *3.4 Characterisation and quantification of flexural fatigue damage*

Fig. 6 illustrates the optical microscopic observation on the external edge surface of the CFRP laminate after 250 cycles in the flexural fatigue test under the normalised CDL $\gamma_c$ = 0.84. Note that the fatigue secant modulus reduced by more than 40%. The damage on the surface occurs near the midspan portion of the specimen in the 1$^{st}$ ply group which is in the compressive stress state. The damaged portion was scanned in the x-ray microtomography to reveal the details of the damage within the specimen (refer to Fig. 7). In the μXT image, the surrounding composite material was removed to better visualise the various damage features. Moreover, the depth of the reconstructed volume was stretched with the in-house algorithm such that the spatial resolution in the depth direction was approximately three times better than that in the length (and width) direction, with the voxel size 8 versus 28 (24) μm (Fig. 7) [27, 28].

As shown in Fig. 7, the damage in the CFRP laminate after 250 flexural fatigue cycles under the $\gamma_c$ = 0.84 comprises transverse cracks (yellow), delamination (blue) and fibre failure (red). The transverse cracks form in the -45 and 0 plies of the 1$^{st}$ ply group along the corresponding fibre direction. Note that the transverse crack includes matrix cracking and matrix/fibre debonding, both of which cannot be differentiated in the μXT image due to the limited resolution and the small fibre diameter. The large delamination occurs at the -45/0 and 0/+45 interfaces while the small delamination at the +45/-45 interface (Fig. 7(b)). The large delamination extends through the entire width; and the delamination tip is irregular. According to the beam theory and the classic laminate theory, in the laminate that consists of plies with different fibre

directions, the strain varies continuously across the depth of the specimen; but the stress, being a function of both the strain and the elastic modulus, exhibits discontinuities through the specimen depth. The high interlaminar shear stress thus arises at the interface between two adjacent plies, and results in the delamination in the specimen. The compressive stress in the 1st ply group gives rise to fibre failure (kinking) across the entire thickness and width (Fig. 7(a) and (c)).

The delamination at the +45/-45, -45/0 and 0/+45 interfaces in the 1st ply group is the predominant failure mode in the CFRP laminate subjected to flexural fatigue. The delamination was projected to the longitudinal plane, and the projected area was then quantitatively estimated using ImageJ software. Fig. 8 shows the delamination area at the three interfaces. The delamination at the -45/0 and 0/+45 interfaces is larger compared to that at the +45/-45 interface because the crack propagation is likely faster in the two interfaces adjacent to the 0 ply in which the fibre fracture leads to the reduced load carrying capacity. The strain energy release rate could be higher at the 0/+45 interface due to the relatively higher interlaminar shear stress, thus resulting in the largest delamination among the three interfaces. Note that further investigation will be performed to track and quantify the 3D damage in the CFRP laminate in various cycle stages of flexural fatigue tests.

## *3.5 Fatigue failure mechanisms*

Fig. 9 shows the typical interlaminar fracture surfaces at the +45/-45, -45/0 and 0/+45 interfaces in the 1st ply group of the CFRP laminate as examined in the SEM after the flexural fatigue tests. Large quantities of fibres are exposed in these fracture surfaces, thus suggesting the matrix/fibre debonding. The fractured epoxy also dominates in the fracture surfaces as demonstrated by the different morphologies in

Fig. 9, such as ridges/valleys, strip-shaped epoxy, shear cusps and abraded epoxy. Therefore, the delamination propagates along the matrix/fibre interface as well as within the epoxy matrix [32]. However, the quantity of exposed fibres seems to be more than the fracture epoxy (Fig. 9); this implies that the matrix/fibre interface is weaker than the interlaminar epoxy in the CFRP in the present study.

The SEM examination also reveals the occurrence of fibre fracture in the 0 ply (refer to Fig. 9(b) and (c)). Shear cups form on the fracture surface as a result of extensive local yielding of the matrix (Fig. 9(b)). The frictional interaction of two adjacent plies under the cyclic load causes the fine epoxy debris especially in the 0 plies (Fig. 9(b) and (c)) and the abrasion of the epoxy matrix, e.g., on the surface of the +45 ply as in Fig. 9(c).

## 4 Conclusions

The stiffness degradation and the fatigue life were investigated on the $[+45/-45/0]_{2s}$ CFRP laminated composites subjected to flexural fatigue loads. X-ray microtomography and fractography were then performed to characterise the 3D fatigue damage and the associated failure mechanism. The conclusions were drawn as follows.

- The flexural fatigue life at failure can be quantitatively determined by the cycle when the tracked secant modulus degrades by 21%. The two-parameter Weibull distribution well represents the statistical nature of the fatigue life data of the CFRP laminate. Combined with the Sigmoidal model, the Weibull analysis method reliably predicts the fatigue life as a function of the applied deflection level.

- The 3D damage in the CFRP laminate consists of matrix cracks, matrix/fibre debonding, fibre failure and delamination. The delamination at the interfaces in the 1st ply group is the predominant failure mode for the flexural fatigue. The delamination area at the -45/0 and 0/+45 interfaces both adjacent to the 0 ply is larger than the delamination area at the +45/-45 interface. Matrix/fibre debonding is the primary mechanism for delamination propagation, while matrix cracking the secondary mechanism.

The flexural fatigue behaviour such as the fatigue life and 3D damage in the $[+45/-45/0]_{2s}$ CFRP laminated composites, as revealed in the present work, provides the insights into the behaviour of laminates with similar layup sequence (i.e., three ply orientations) for some parts in the wind turbine blade.

## Acknowledgements

This work was financially supported by the Ministry of Defence Singapore – Nanyang Technological University (NTU) Joint Applied R&D Cooperation (JPP) Programme (Grant No.: MINDEF-NTU-JPP/12/01/02). ZL acknowledges the NTU Interdisciplinary Graduate School Research Student Scholarship.

## References

[1] Veers PS, Ashwill TD, Sutherland HJ, Laird DL, Lobitz DW, Griffin DA, et al. Trends in the design, manufacture and evaluation of wind turbine blades. Wind Energy. 2003;6(3):245-59.

[2] Ashwill TD. Materials and innovations for large blade structures: research opportunities in wind energy technology. In: Proceedings of 50th AIAA/ASME/ASCE/AHS/ASC Structures, Structural Dynamics, and Materials Conference. Palm Springs, Conference, Conference 2009.

[3] Meng M, Rizvi MJ, Grove SM, Le HR. Effects of hygrothermal stress on the failure of CFRP composites. Compos Struct. 2015;133:1024-35.

[4] Kensche CW. Fatigue of composites for wind turbines. Int J Fatigue. 2006;28(10):1363-74.
[5] Sakin R, Ay I, Yaman R. An investigation of bending fatigue behavior for glass-fiber reinforced polyester composite materials. Mater Des. 2008;29(1):212-7.
[6] Liu BY, Lessard LB. Fatique and damage-tolerance analysis of composite laminates: Stiffness loss, damage-modelling, and life prediction. Compos Sci Technol. 1994;51(1):43-51.
[7] Belingardi G, Cavatorta MP. Bending fatigue stiffness and strength degradation in carbon-glass/epoxy hybrid laminates: Cross-ply vs. angle-ply specimens. Int J Fatigue. 2006;28(8):815-25.
[8] Philippidis TP, Vassilopoulos AP. Fatigue of composite laminates under off-axis loading. Int J Fatigue. 1999;21(3):253-62.
[9] Jessen SM, Plumtree A. Continuum damage mechanics applied to cyclic behaviour of a glass fibre composite pultrusion. Composites. 1991;22(3):181-90.
[10] Jones CJ, Dickson RF, Adam T, Reiter H, Harris B. Environmental fatigue of reinforced plastics. Composites. 1983;14(3):288-93.
[11] Bedi R, Chandra R. Fatigue-life distributions and failure probability for glass-fiber reinforced polymeric composites. Compos Sci Technol. 2009;69(9):1381-7.
[12] Philippidis TP, Vassilopoulos AP. Fatigue design allowables for GRP laminates based on stiffness degradation measurements. Compos Sci Technol. 2000;60(15):2819-28.
[13] Tai NH, Ma CCM, Wu SH. Fatigue behaviour of carbon fibre/PEEK laminate composites. Composites. 1995;26(8):551-9.
[14] Lambert J, Chambers AR, Sinclair I, Spearing SM. 3D damage characterisation and the role of voids in the fatigue of wind turbine blade materials. Compos Sci Technol. 2012;72(2):337-43.
[15] Kar NK, Barjasteh E, Hu Y, Nutt SR. Bending fatigue of hybrid composite rods. Compos Part A. 2011;42(3):328-36.
[16] Salvia M, Fiore L, Fournier P, Vincent L. Flexural fatigue behaviour of UD GFRP experimental approach. Int J Fatigue. 1997;19(3):253-62.
[17] Li P. Constitutive and failure behaviour in selective laser melted stainless steel for microlattice structures. Mater Sci Eng A. 2015;622:114-20.
[18] Huang R, Li P, Liu T. X-ray microtomography and finite element modelling of compressive failure mechanism in cenosphere epoxy syntactic foams. Compos Struct. 2016;140:157-65.
[19] Li P, Lee PD, Lindley TC, Maijer DM, Davis GR, Elliott JC. X-ray microtomographic characterisation of porosity and its influence on fatigue crack growth. Adv Eng Mater. 2006;8(6):476-9.

[20] Tan KT, Watanabe N, Iwahori Y. X-ray radiography and micro-computed tomography examination of damage characteristics in stitched composites subjected to impact loading. Compos Part B. 2011;42(4):874-84.
[21] McCombe GP, Rouse J, Trask RS, Withers PJ, Bond IP. X-ray damage characterisation in self-healing fibre reinforced polymers. Compos Part A. 2012;43(4):613-20.
[22] Hufenbach W, Boehm R, Gude M, Berthel M, Hornig A, Rucevskis S, et al. A test device for damage characterisation of composites based on in situ computed tomography. Compos Sci Technol. 2012;72(12):1361-7.
[23] Moffat AJ, Wright P, Buffiere JY, Sinclair I, Spearing SM. Micromechanisms of damage in 0° splits in a [90/0]s composite material using synchrotron radiation computed tomography. Scr Mater. 2008;59(10):1043-6.
[24] Chambers AR, Earl JS, Squires CA, Suhot MA. The effect of voids on the flexural fatigue performance of unidirectional carbon fibre composites developed for wind turbine applications. Int J Fatigue. 2006;28(10):1389-98.
[25] Meng M, Le HR, Rizvi MJ, Grove SM. 3D FEA modelling of laminated composites in bending and their failure mechanisms. Compos Struct. 2015;119:693-708.
[26] Li P, Petrinic N, Siviour CR. Microstructure and x-ray microtomographic characterisation of deformation in electrodeposited nickel thin-walled hollow spheres. Mater Lett. 2013;100:233-6.
[27] Liu T. Cone-beam CT reconstruction for planar object. NDT&E Int. 2012;45(1):9-15.
[28] Liu T, Huang R, Li P. Cone-beam CT reconstruction along any orientation of interest. J X-Ray Sci Technol. 2015;23(6):773-82.
[29] Tate JS, Kelkar AD. Stiffness degradation model for biaxial braided composites under fatigue loading. Compos Part B. 2008;39(3):548-55.
[30] Tserpes KI, Papanikos P, Labeas G, Pantelakis S. Fatigue damage accumulation and residual strength assessment of CFRP laminates. Compos Struct. 2004;63(2):219-30.
[31] Neville AM, Kennedy JB. Basic statistical methods for engineers and scientists: International Textbook; 1964.
[32] Hibbs MF, Bradley WL. Correlations between micromechanical failure processes and the delamination toughness of graphite/epoxy systems. In: Masters JE, Au JJ, editors. Fractography of modern engineering materials: composites and metals, ASTM STP 948: ASTM; 1987. p. 68-97.

## List of Tables

Table 1 The flexural properties of CFRP laminates subjected to static three-point bending and subsequent reloading.

| Initial modulus (GPa) | Flexural strength (MPa) | Flexural failure deflection (mm) | Residual modulus (GPa) | Residual strength (MPa) |
|---|---|---|---|---|
| 28.1±0.8 | 872±24 | 14.4±0.5 | 22.2±2.9 | 542±41 |

Table 2 The Weibull parameters for the flexural fatigue life distribution of CFRP laminates under different normalised CDL ($\gamma_c$).

| $\gamma_c$ = CDL/SFD | Shape parameter, $\alpha$ | Scale parameter, $\beta$ | Correlation coefficient |
|---|---|---|---|
| 0.91 | 0.8051 | 55 | 0.9276 |
| 0.84 | 0.7811 | 382 | 0.9466 |
| 0.71 | 0.5104 | 3206 | 0.9361 |
| 0.65 | 0.6925 | 57236 | 0.9494 |
| 0.58 | 0.9622 | 394784 | 0.9587 |

Table 3 Kolmogorov-Smirnov goodness-of-fit test results for Weibull analysis of the flexural fatigue life distribution of CFRP laminates under different normalised CDL ($\gamma_c$).

| $\gamma_c$ = CDL/SFD | Goodness-of-fit statistic, $D$ | Critical value, $D_c$ | $D < D_c$? |
|---|---|---|---|
| 0.91 | 0.189 | 0.454 | Yes |
| 0.84 | 0.151 | 0.454 | Yes |
| 0.71 | 0.178 | 0.454 | Yes |
| 0.65 | 0.212 | 0.454 | Yes |
| 0.58 | 0.139 | 0.454 | Yes |

## List of Figures

Fig. 1 Optical image of the polished transverse cross section of the +45 ply in the $[+45/-45/0]_{2s}$ CFRP laminate.

Fig. 2 The representative flexural stress–strain curves of CFRP laminates subjected static three-point bending and subsequent reloading.

Fig. 3 The variation of the normalised stiffness with the number of cycles under different normalised CDL ($\gamma_c$).

Fig. 4 The flexural fatigue life distribution of CFRP laminates under different normalised CDL ($\gamma_c$) fitted using the Weibull model.

Fig. 5 The predicted fatigue life at three failure probabilities under different normalised CDL ($\gamma_c$) and the normalised $\gamma_c$ versus fatigue life curves fitted using the Sigmoidal model.

Fig. 6 Optical image of the CFRP laminate after 250 cycles in the flexural fatigue test under the normalised CDL $\gamma_c = 0.84$.

Fig. 7 X-ray microtomographic observations of the damages in the CFRP laminate after 250 cycles in the flexural fatigue test under the normalised CDL $\gamma_c = 0.84$. Transverse cracks and fibre failure in the 1st ply group are denoted in (a) while the delamination is in (b). The delamination at the -45/0 interface is hidden in (c) to better illustrate the damage in the 0 ply.

Fig. 8 Projected delamination area at the different interfaces in the 1st ply group after 250 cycles in the flexural fatigue test under the normalised CDL $\gamma_c = 0.84$.

Fig. 9 SEM images of the fracture surfaces in the ply interfaces in the 1$^{st}$ and 2$^{nd}$ groups. Note that the scale bar as indicated in (a) applies to all SEM images.

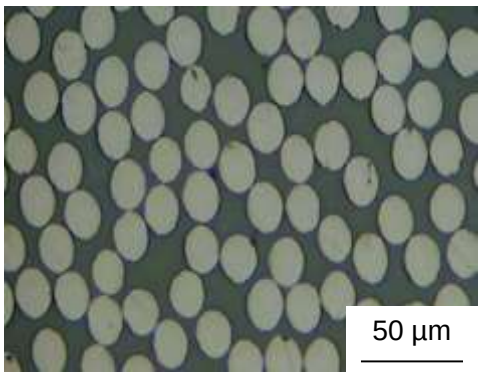


Figure 1: Optical image of the polished transverse cross section of the +45 ply in the $[+45/-45/0]_{2s}$ CFRP laminate.

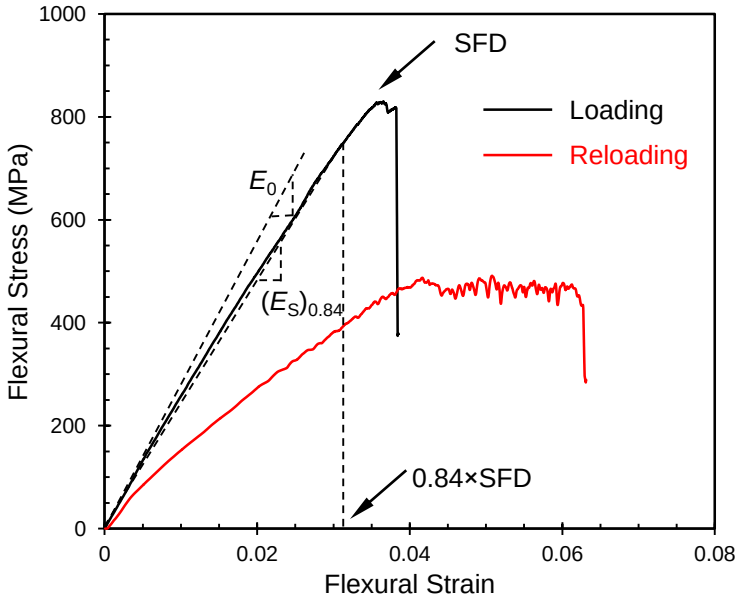


Figure 2: The representative flexural stress–strain curves of CFRP laminates subjected static three-point bending and subsequent reloading.

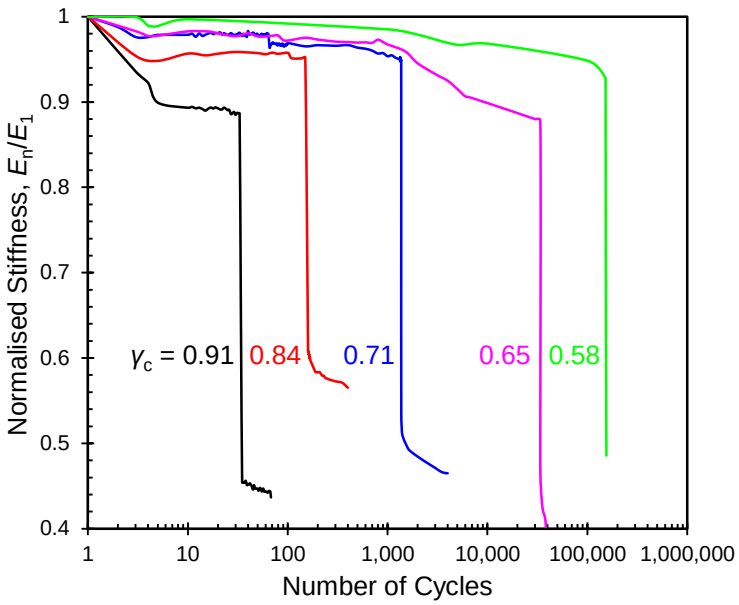


Figure 3: The variation of the normalised stiffness with the number of cycles under different normalised CDL ($\gamma_c$).

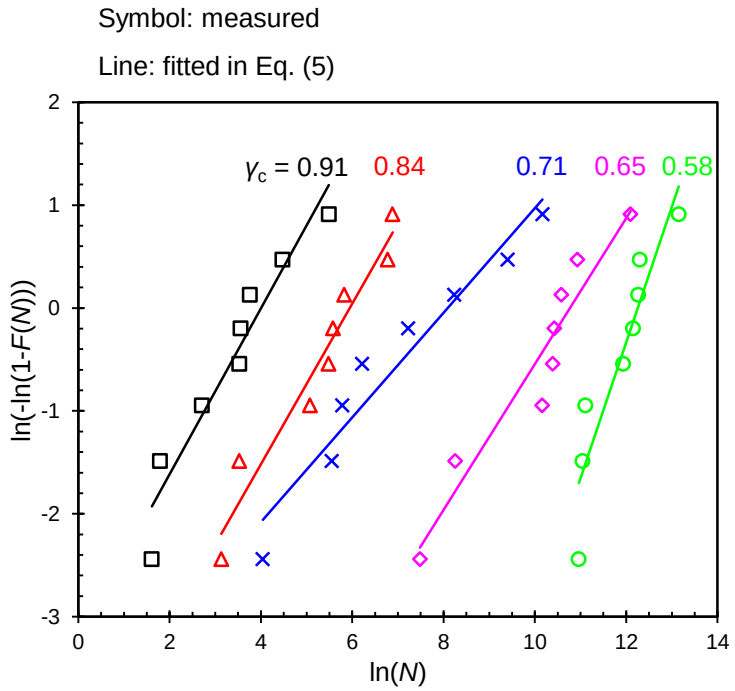


Figure 4: The flexural fatigue life distribution of CFRP laminates under different normalised CDL ($\gamma_c$) fitted using the Weibull model.

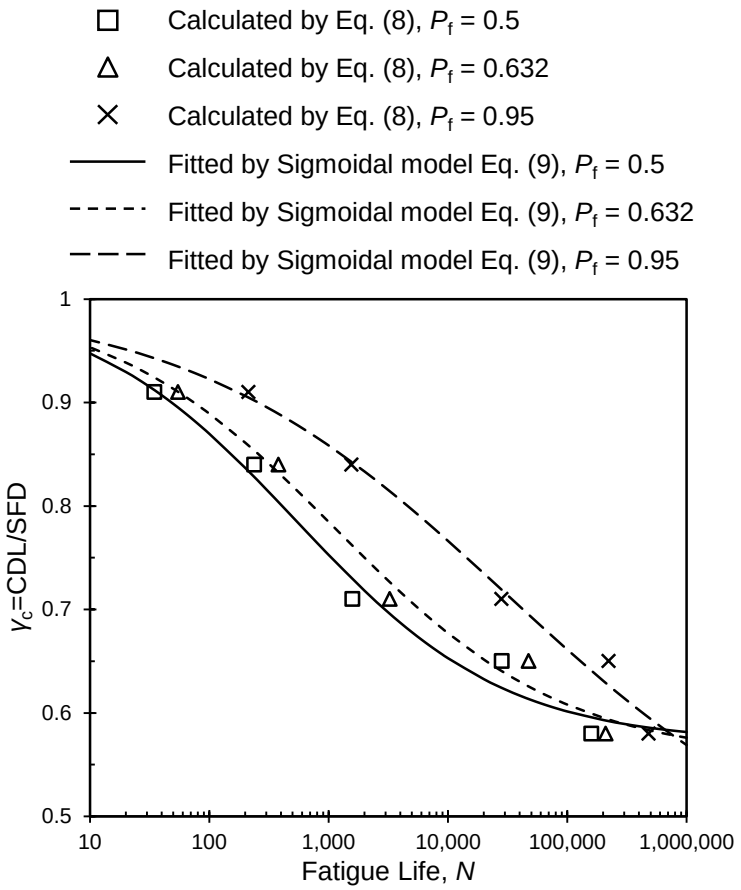


Figure 5: The predicted fatigue life at three failure probabilities under different normalised CDL ($\gamma_c$) and the normalised $\gamma_c$ versus fatigue life curves fitted using the Sigmoidal model.

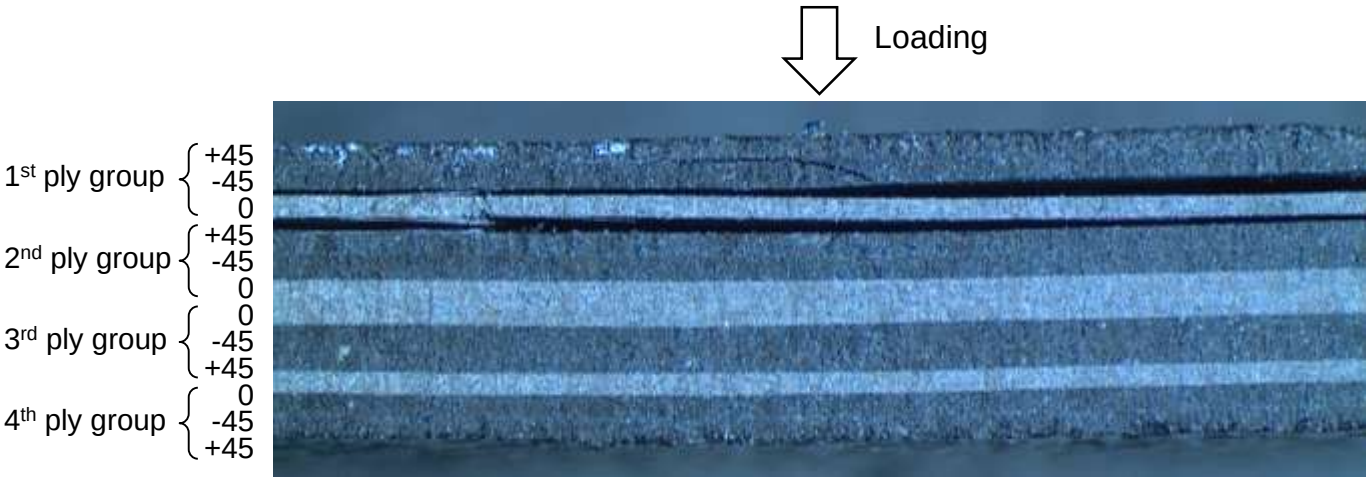


Figure 6: Optical image of the CFRP laminate after 250 cycles in the flexural fatigue test under the normalised CDL $\gamma_c$ = 0.84.

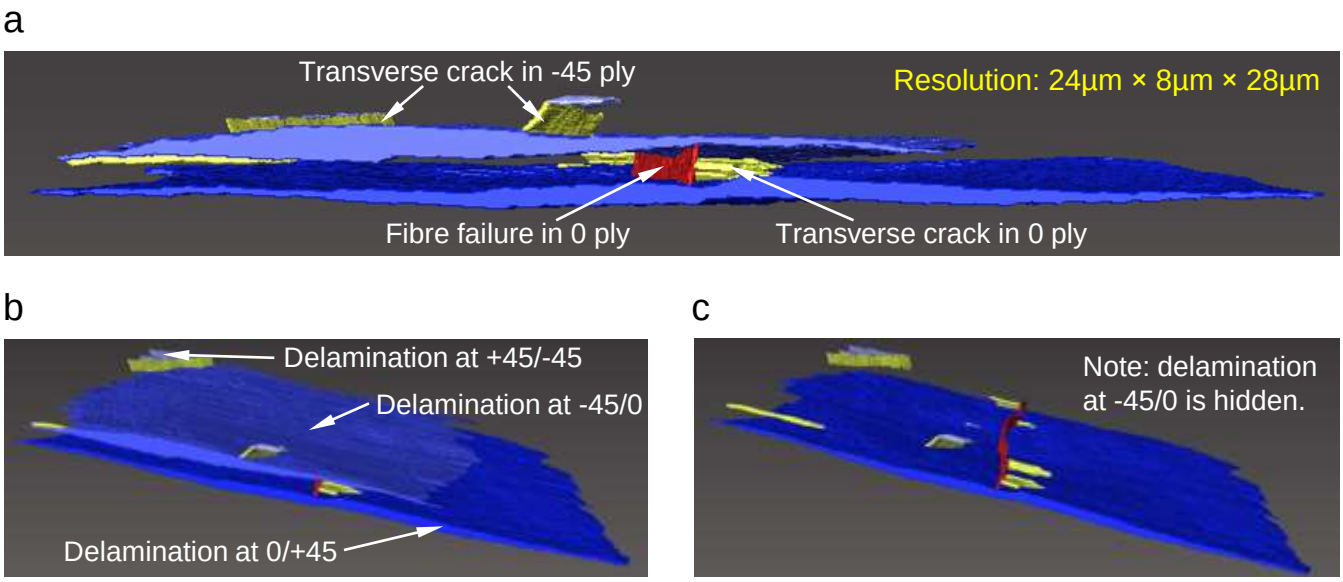


Figure 7: X-ray microtomographic observations of the damages in the CFRP laminate after 250 cycles in the flexural fatigue test under the normalised CDL $\gamma_c$ = 0.84. Transverse cracks and fibre failure in the 1st ply group are denoted in (a) while the delamination is in (b). The delamination at the -45/0 interface is hidden in (c) to better illustrate the damage in the 0 ply.

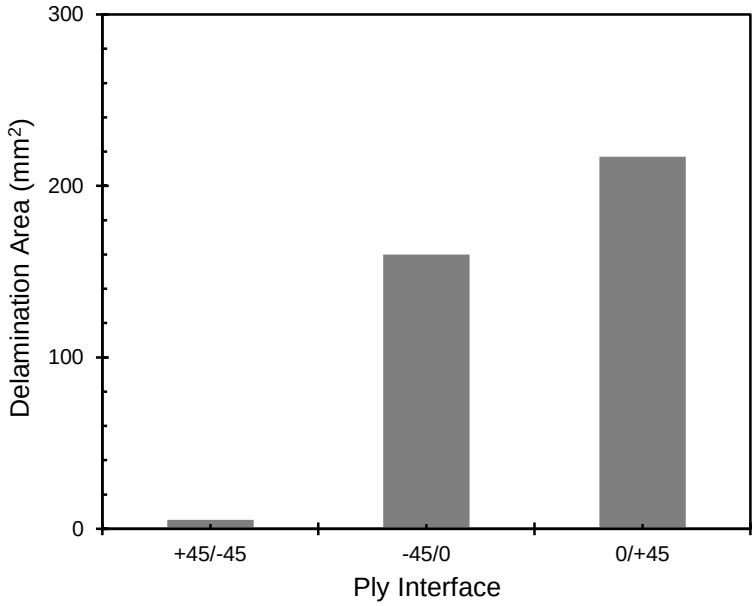


Figure 8: Projected delamination area at the different interfaces in the 1st ply group after 250 cycles in the flexural fatigue test under the normalised CDL $\gamma_c$ = 0.84.

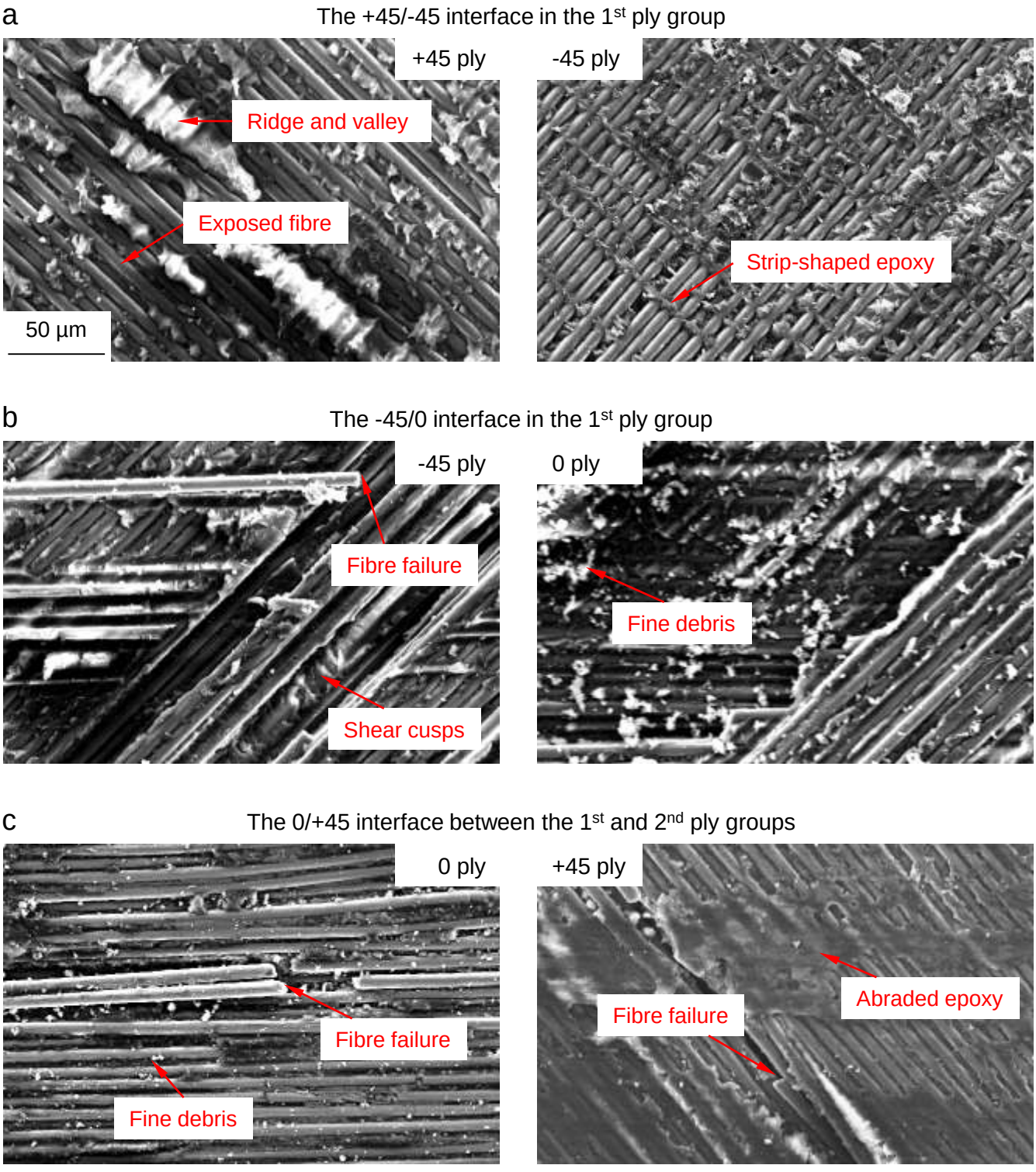


Figure 9: SEM images of the fracture surfaces in the ply interfaces in the 1st and 2nd groups. Note that the scale bar as indicated in (a) applies to all SEM images.